# Description of Aromaticity with the Help of Vibrational Spectroscopy: Anthracene and Phenanthrene

Robert Kalescky, Elfi Kraka, and Dieter Cremer*

Computational and Theoretical Chemistry Group (CATCO), Department of Chemistry, Southern Methodist University, 3215 Daniel Avenue, Dallas, Texas 75275-0314, United States

Ⓢ Supporting Information

ABSTRACT: A new approach is presented to determine π-delocalization and the degree of aromaticity utilizing measured vibrational frequencies. For this purpose, a perturbation approach is used to derive vibrational force constants from experimental frequencies and calculated normal mode vectors. The latter are used to determine the local counterparts of the vibrational modes. Next, relative bond strength orders (RBSO) are obtained from the local stretching force constants, which provide reliable descriptors of CC and CH bond strengths. Finally, the RBSO values for CC bonds are used to establish a modified harmonic oscillator model and an aromatic delocalization index AI, which is split into a bond weakening (strengthening) and bond alternation part. In this way, benzene, naphthalene, anthracene, and phenanthrene are described with the help of vibrational spectroscopy as aromatic systems with a slight tendency of peripheral π-delocalization. The 6.8 kcal/mol larger stability of phenanthrene relative to anthracene predominantly (84%) results from its higher resonance energy, which is a direct consequence of the topology of ring annelation. Previous attempts to explain the higher stability of phenanthrene via a maximum electron density path between the bay H atoms are misleading in view of the properties of the electron density distribution in the bay region.
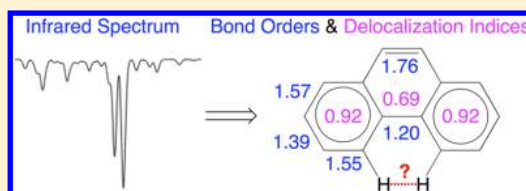
INTRODUCTION

The description of the chemical bond is one of the major objectives in chemistry. The large variety of atom—atom interactions, which reaches from strong covalent to weak electrostatic interactions has been investigated with both experimental and quantum chemical, i.e., computational tools.[1−3] Special focus has been on the description of bonding in cyclic conjugated systems, which obtain via π-electron delocalization special properties. The conceptual approach to the description of these systems is summarized under the terms aromaticity and antiaromaticity.[4−9]

There are numerous experimental and computational investigations of aromatic or antiaromatic π-electron systems. A quantification of the (anti)aromatic character of a molecule with the help of its stability (energy), structure (geometry), reactivity, or spectroscopic properties fills myriads of primary and secondary articles, only some of which can be mentioned here.[4−10] However, most investigations on aromaticity have been based on calculated rather than measured quantities. This has to do with limitations faced by experiments.

Stability measurements of destabilized antiaromatic compounds are difficult and, apart from this, measured energies are not accurate enough to detect some of the finer effects of electron delocalization in distorted, strained, or charged cyclic π-systems. Molecular parameters such as bond lengths provide a better account of structural changes caused by (anti)aromaticity; however, X-ray, r_0, r_a, r_z etc. geometries are difficult to compare apart from the problem that bond lengths are not reliable bond strength and π-delocalization descriptors.[11] Much work has been carried out utilizing the magnetic properties;[4,7,9] however, the

NMR chemical shift of an atomic nucleus is also affected by more than just π-delocalization effects. Similarly, NMR spin—spin coupling constants are inappropriate measures for a change in the bond strength as caused by π-delocalization.[12]

Up to this time, the vibrational properties of a molecule have hardly been used to describe the aromatic or antiaromatic character of a conjugated cyclic molecule in a systematic way.[13,14] In view of the high accuracy, by which, e.g., vibrational frequencies can be measured, they should provide a sensitive measure for the degree of π-delocalization and thereby also aromaticity in a molecule. Of course, one could argue that for antiaromatic and thereby destabilized molecules, the measurement of vibrational properties is as difficult as that of other molecular properties. However, low temperature matrix isolation spectroscopy[15] makes the measurement of vibrational spectra of labile compounds possible. Also, reliable vibrational frequencies can conveniently be calculated as second-order response properties and, when augmented by anharmonicity corrections,[16,17] they are close to experimental frequencies.

There is, however, the argument that vibrational frequencies are not suitable descriptors because they depend on atomic masses and cannot be associated with special bonds because the vibrational normal modes are delocalized over the framework of the molecule as a result of mode—mode coupling.[11,18−20] In this work, we will show that both problems can be solved and that measured experimental frequencies provide an excellent tool for
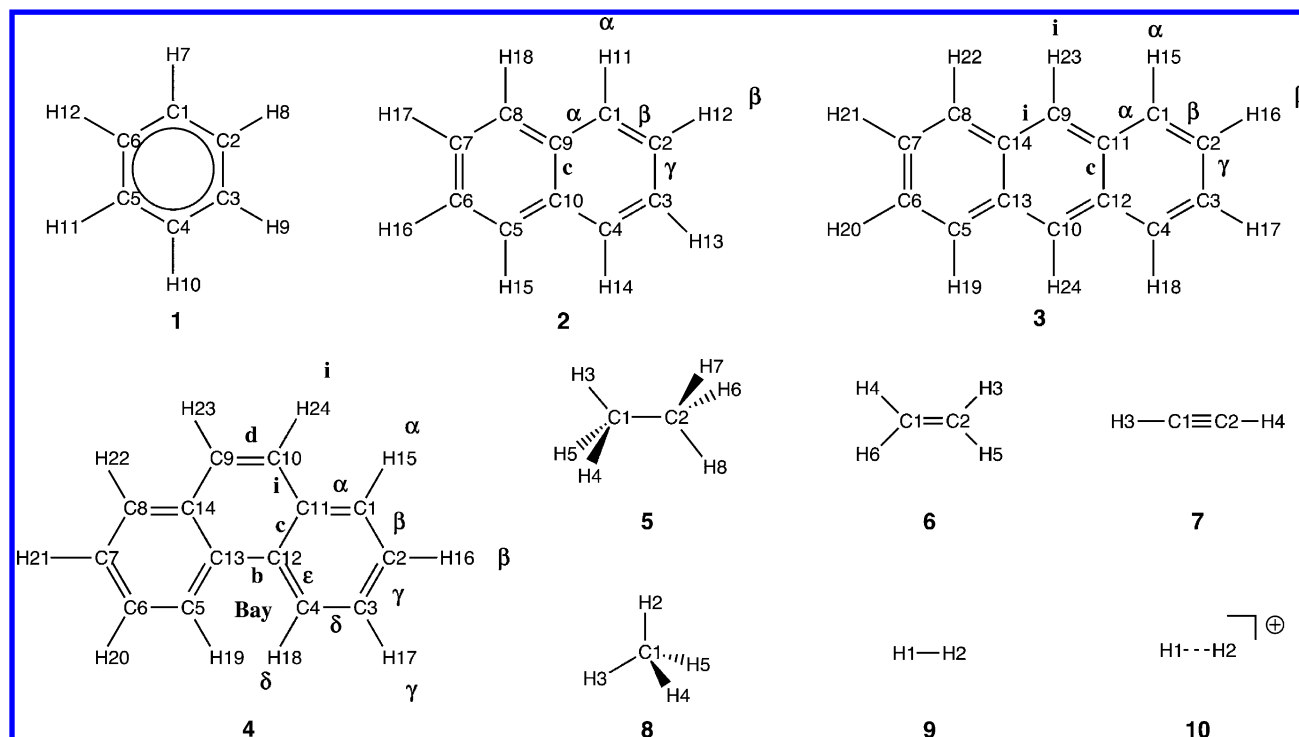
Figure 1. Target and reference molecules with numbering of atoms. For simplifying the discussion, specific CH and CC bonds are denoted as i (inner), c (central), b (bridge), or by Greek symbols.

describing the aromatic character of a molecule. We will investigate benzene (**1**) and the benzoid polycyclic hydrocarbons naphthalene (**2**), anthracene (**3**), and phenanthrene (**4**) (see Figure 1), for which all $3N - 6 = N_{vib}$ (N: number of atoms) vibrational frequencies have been measured.[21−29] We will demonstrate that by (i) using vibrational frequencies to determine an experimentally based force constant matrix, (ii) using the force constants and auxiliary calculations to extract local vibrational modes, which can be assigned to individual bonds, and (iii) determining local stretching force constants based on the experimental frequencies, which are no longer flawed by mass effects or mode−mode coupling, we obtain a sensitive measure for the strength of the chemical bonds in a cyclic conjugated molecule as it results from π-delocalization.

A local stretching mode[30,31] probes the strength of a bond by distorting it without changing its electronic structure. As a matter of fact, its stretching force constant and frequency relate to an infinitesimal change of the bond. The force constant reflects the curvature of the adiabatic Born−Oppenheimer potential energy surface (PES) in the direction of the internal coordinate with which it is associated. As long as the Born−Oppenheimer approximation is appropriate, which is the case for all molecules investigated in this work, the local stretching force constants provide excellent bond strength descriptors as was shown in previous work.[31−36]

Once a set of bond strength descriptors in the form of stretching force constants has been derived from the experimental frequencies, these can be converted for easier use into relative bond strength orders (RBSO) choosing appropriate reference bonds. The RBSO values can be applied in connection with the Harmonic Oscillator Model of Aromaticity (HOMA)[37−40] to determine the degree of aromaticity. Furthermore, we will investigate the question of whether the interactions between the CH bonds of the bay region of phenanthrene leads to any stabilization and whether this is the cause for its increased stability compared to that of anthracene.[41−45]

In this work, we will demonstrate that vibrational spectroscopy can provide reliable information about aromatic molecules. The results of this work will be presented in the following way. In Section 2, the computational methods and details will be described. The normal and local vibrational frequencies of the target molecules will be discussed in Section 3, whereas in Section 4 RBSO and HOMA parameters for the analysis of the aromatic character of the target molecules will be presented. Finally, in Section 5, the conclusions of this work will be summarized.

■ COMPUTATIONAL METHODS

Experimental frequencies for benzene,[21] naphthalene,[22] anthracene,[23−28] and phenanthrene[29] as well as the reference molecules methane,[21] ethane,[21] ethene,[21] and acetylene[21] were taken from the literature. The force constant matrix associated with a complete set of $3N - 6$ vibrational frequencies can be determined utilizing the Wilson equation of vibrational spectroscopy:[18]

$$\mathbf{F}^q \mathbf{D} = \mathbf{G}^{-1}\mathbf{D}\mathbf{\Lambda} \tag{1}$$

where $\mathbf{F}^q$ is the calculated force constant matrix expressed in internal coordinates q_n, $\mathbf{D}$ collects the vibrational eigenvectors $\mathbf{d}_\mu$ in form of column vectors ($\mu = 1, \cdots, N_{vib}$ with $N_{vib} = 3N - L$; N: number of atoms; L: number of translations and rotations), $\mathbf{G}$ is the Wilson matrix for the kinetic energy,[18] and $\mathbf{\Lambda}$ is a diagonal matrix containing the vibrational eigenvalues $\lambda_\mu = 4\pi^2 c^2 \omega_\mu^2$. In the expression for the eigenvalues, ω_μ represents the vibrational frequency of mode $\mathbf{d}_\mu$. Matrix $\mathbf{G}$ can be determined with the help of the atomic masses and the $\mathbf{B}$ matrix

$$\mathbf{G} = \mathbf{B}\mathbf{M}^{-1}\mathbf{B}^\dagger \tag{2}$$

where $\mathbf{B}$ is a rectangular ($N_{vib} \times 3N$) matrix containing the first derivatives of the internal coordinates with regard to the

Cartesian coordinates. Hence, the force constant matrix $\mathbf{F}^q$ associated with the experimental frequencies can only be determined if, by an appropriate quantum chemical calculation, the normal mode vectors collected in the matrix $\mathbf{D}'$ are determined. Clearly, the true mode matrix $\mathbf{D}$ will differ from the calculated matrix $\mathbf{D}'$. However, test calculations with different quantum chemical methods reveal that the influence of the matrix $\mathbf{D}'$ on final results obtained in form of the local mode frequencies is relatively small and does not exceed 10 cm^{-1}. However, this requires that the quantum chemical calculation reproduces the correct ordering of the normal-mode frequencies as found experimentally and that the symmetries of the calculated normal mode vectors comply with those assigned to the experimental frequencies.

These requirements are fulfilled for the target molecules by using the DFT (density functional theory) functional B3LYP[46,47] and the aug-cc-pVTZ basis set of Dunning.[48,49] When calculating the normal mode vectors of a molecule, normal-mode frequencies and force constants are obtained. These differ from the experimental ones as expressed in eq 3:[19]

$$(\mathbf{F}'^q + \Delta\mathbf{F}^q)\mathbf{D}' = \mathbf{G}^{-1}\mathbf{D}'(\boldsymbol{\Lambda}' + \Delta\boldsymbol{\Lambda}) \tag{3}$$

where $\mathbf{F}'^q$ and $\boldsymbol{\Lambda}'$ are based on the quantum chemical calculations. The diagonal matrix $\Delta\boldsymbol{\Lambda}$ is defined by the differences $\omega_\mu^{cal} - \omega_\mu^{exp}$. Hence, the unknown perturbation matrix $\Delta\mathbf{F}^q$ can be obtained from eq 4:

$$\Delta\mathbf{F}^q\mathbf{D}' = \mathbf{G}^{-1}\mathbf{D}'\Delta\boldsymbol{\Lambda} \tag{4}$$

By defining $\tilde{\mathbf{D}} = \mathbf{G}^{-1/2}\mathbf{D}'$, which leads to $\tilde{\mathbf{D}}^\dagger\tilde{\mathbf{D}} = \tilde{\mathbf{D}}\,\tilde{\mathbf{D}}^\dagger = \mathbf{I}$ and setting $\Delta\tilde{\mathbf{F}} = \mathbf{G}^{1/2}\Delta\mathbf{F}\mathbf{G}^{1/2}$, an eigenvalue problem can be defined according to

$$\Delta\tilde{\mathbf{F}}\tilde{\mathbf{D}} = \tilde{\mathbf{D}}\Delta\boldsymbol{\Lambda} \tag{5}$$

which is solved by diagonalization. In this way $\Delta\tilde{\mathbf{F}}$ and $\Delta\mathbf{F}$ are obtained that lead directly to the force constant matrix $\mathbf{F}^q$ corresponding to the experimental frequencies.

The local vibrational modes are obtained by diagonalizing the force constant matrix $\mathbf{F}^q$, which yields matrix $\mathbf{K}$, and then calculating the local mode vectors $\mathbf{a}_n$ related to internal coordinate q_n:[30−32]

$$\mathbf{a}_n = \frac{\mathbf{K}^{-1}\mathbf{d}_n^\dagger}{\mathbf{d}_n\mathbf{K}^{-1}\mathbf{d}_n^\dagger} \tag{6}$$

where $\mathbf{d}_n$ is a row vector of matrix $\mathbf{D}$. The local mode force constant k_n^a is given by eq 7:

$$k_n^a = \mathbf{a}_n^\dagger\mathbf{K}'\mathbf{a}_n \tag{7}$$

and the local mode frequency ω_n^a can be obtained from

$$(\omega_n^a)^2 = \frac{G_{nn}k_n^a}{4\pi^2c^2} \tag{8}$$

where element G_{nn} of matrix $\mathbf{G}$ defines the local mode mass.[30]

The relationship between local and normal frequencies is determined in an adiabatic connection scheme (ACS),[31] which can be obtained by rewriting the Wilson equation (eq 1) with the help of the compliance matrix $\boldsymbol{\Gamma}^q = (\mathbf{F}^q)^{-1}$ as[31,32]

$$\mathbf{G}(\boldsymbol{\Gamma}^q)^{-1}\mathbf{D} = \mathbf{D}\boldsymbol{\Lambda}$$

$$\mathbf{G}\mathbf{R} = \boldsymbol{\Gamma}^q\mathbf{R}\boldsymbol{\Lambda} \tag{9}$$

where the new eigenvector matrix $\mathbf{R}$ is given by $(\boldsymbol{\Gamma}^q)^{-1}\mathbf{D}$. Zou and co-workers[31,32] partitioned matrices $\boldsymbol{\Gamma}^q$ and $\mathbf{G}$ into diagonal ($\boldsymbol{\Gamma}_d^q$ and $\mathbf{G}_d$) and off-diagonal ($\boldsymbol{\Gamma}_o^q$ and $\mathbf{G}_o$) parts:

$$(\mathbf{G}_d + \lambda\mathbf{G}_o)\mathbf{R}_\lambda = (\boldsymbol{\Gamma}_d^q + \lambda\boldsymbol{\Gamma}_o^q)\mathbf{R}_\lambda\boldsymbol{\Lambda}_\lambda \tag{10}$$

The scaling factor λ varies from 0 to 1. For $\lambda = 0$, the local vibrational modes are obtained, whereas $\lambda = 1$ defines the normal vibrational modes. Equation 10 is the basis for the ACS, which, by increasing parameter λ stepwise from 0 to 1, relates local vibrational modes to normal vibrational modes in terms of their eigenvalues (frequencies) and eigenvectors (mode vectors).[31,32] In this way, each normal-mode frequency ω_μ can be expressed by a local mode frequency ω_a and a coupling frequency ω_c, i.e., $\omega_\mu = \omega_a + \omega_c$. The zero-point energy (ZPE) is split up in two parts where one results from the local mode frequencies (ZPE(local)) and the other from the coupling frequencies (ZPE(coup)).[31] If the internal coordinates of the target molecule are properly chosen, ZPE(coup) makes a minimal contribution (<5%) to the total ZPE (ZPE condition).

For an N-atom molecule, the N_{vib} normal vibrational modes are exactly defined, which is, however, not the case for the number of local vibrational modes. For example, the molecule CH_4 has $3N - 6 = 9$ vibrational modes; however, one can choose a redundant coordinate set of 4 bond lengths and 6 bond angles to describe its geometry. When setting up the ACS of methane, using 10 rather than 9 internal coordinates, one of the local mode frequencies associated with the HCH bond angles is reduced to zero for $\lambda \to 1$. In general, an ACS diagram is always constructed from an internal coordinate set for a given molecule. Then, the ACS selects those local modes, which have the strongest overlap with the normal vibrational modes and eliminates all those that are not relevant for the description. In this way, N_{vib} internal coordinates are always defined, which are needed (irrespective of any symmetry) for the description of the molecular geometry and the local vibrational modes.[30] For example in the case of the C-framework of benzene, all dihedral angles but three are eliminated, which is in line with the observation that there are only 3 out-of-plane normal modes.[50,51]

RBSO values for CC bonds were obtained by using as suitable references the local CC stretching force constant of ethane and ethene both derived from experimental frequencies as described above.[21] According to general chemical understanding, these molecules have CC bond orders of 1 and 2, respectively. Utilizing the extended Badger rule,[36,52] we have shown that the RBSO is related to the stretching force constant by a power relationship, which is fully determined by two reference values and the requirement that, for a zero-force constant, the RBSO value must also be zero. In this way, the relationship RBSO(CC) = $a(k^a)^b$ with a(CC) and b(CC) being equal to 0.2991 and 0.8658 was obtained.

For establishing the RBSO(CH) relationship, the extended Badger rule[36] was first applied to determine for F−H bonds a suitable relationship and then adjusting the latter to give for methane an RBSO(CH) value of 1.00. As XH stretching references, the experimental frequencies of F−H[53] (bond order 1) and the $D_{\infty h}$-symmetrical $[\text{F}\cdots\text{H}\cdots\text{F}]^-$[54] (bond order 0.5) were taken. The resulting power relationship for CH bonds is defined by $a = 0.3892$ and $b = 0.5419$.

Originally, the HOMA index[37−40] was based on the concept of an optimal bond length (rather than a mean bond length);

$$\text{HOMA} = 1 - \frac{\alpha}{N_B}\sum(R_{opt} - R_i)^2 \tag{11}$$

Table 1. Experimental Normal Mode Frequencies ω_μ and the Corresponding Local Mode Force Constants k_n^a and Frequencies ω_n^a of Anthracene (3)[a]

μ	sym.	ω_μ [cm^{-1}]	#	parameter	k^a [mdyn Å^{-1}][a]	ω^a [cm^{-1}]	ω_{coup} [cm^{-1}]	μ	sym.	ω_μ [cm^{-1}]	#	parameter	k^a [mdyn Å^{-1}][a]	ω^a [cm^{-1}]	ω_{coup} [cm^{-1}]
66	B_{1u}	3084	6	C6–H20	5.103	3052	32	32	A_u	958	46	H15–C1–C2–H16	0.183	948	10
65	A_g	3072	2	C2–H16	5.103	3052	20	31	B_{3u}	956	51	H21–C7–C8–H22	0.183	948	8
64	B_{3g}	3054	3	C3–H17	5.103	3052	2	30	B_{1g}	956	48	H17–C3–C4–H18	0.183	948	8
63	B_{1u}	3053	1	C1–H15	5.057	3038	15	29	B_{2g}	952	49	H19–C5–C6–H20	0.183	948	4
62	B_{2u}	3048	7	C7–H21	5.103	3052	−4	28	B_{1u}	906	25	C11–C12	5.202	1213	−307
61	A_g	3048	8	C8–H22	5.057	3038	10	27	B_{3g}	903	26	C13–C14	5.202	1213	−310
60	A_g	3027	9	C9–H23	4.990	3018	9	26	B_{2g}	896	50	H20–C6–C7–H21	0.164	884	12
59	B_{2u}	3021	5	C5–H19	5.057	3038	−17	25	B_{3u}	883	61	C1–C11–C9–H23	0.213	785	98
58	B_{3g}	3017	4	C4–H18	5.057	3038	−21	24	A_u	858	47	H16–C2–C3–H17	0.164	884	−26
57	B_{1u}	3007	10	C10–H24	4.990	3018	−11	23	B_{2g}	832	62	C5–C13–C10–H24	0.213	785	47
56	B_{3g}	1632	16	C5–C6	7.307	1438	194	22	B_{2u}	809	32	C12–C10–C13	2.448	948	−139
55	B_{1u}	1620	11	C1–C2	7.307	1438	182	21	B_{2g}	773	65	H15–C1–C11–C12	0.244	732	42
54	B_{3g}	1574	22	C9–C14	6.202	1325	249	20	A_g	754	30	C9–C11–C12	2.448	926	−172
53	A_g	1556	14	C3–C4	7.307	1438	118	19	B_{1g}	747	66	H19–C5–C13–C14	0.244	732	16
52	B_{2u}	1534	19	C7–C8	7.307	1438	96	18	A_u	743	55	C9–C11–C12–C10	0.389	594	149
51	A_g	1480	21	C9–C11	6.202	1325	155	17	B_{3u}	737	57	C12–C10–C13–C14	0.350	583	154
50	B_{2u}	1460	24	C10–C13	6.202	1325	135	16	B_{1u}	653	35	C6–C5–C13	2.310	920	−267
49	B_{1u}	1448	23	C10–C12	6.202	1325	123	15	A_g	625	31	C11–C12–C10	2.448	926	−301
48	A_g	1412	44	H23–C9–C14	0.893	1265	148	14	B_{2u}	601	27	C1–C2–C3	2.179	893	−292
47	B_{2u}	1397	45	H24–C10–C12	0.893	1265	133	13	B_{2g}	580	52	C1–C2–C3–C4	0.346	589	−9
46	B_{3g}	1372	39	H18–C4–C12	0.882	1254	118	12	A_u	552	56	C11–C12–C10–C13	0.350	583	−31
45	B_{2u}	1346	40	H19–C5–C6	0.873	1256	90	11	B_{3g}	522	29	C3–C4–C12	2.310	920	−398
44	B_{1u}	1317	43	H22–C8–C14	0.882	1254	63	10	B_{1g}	479	58	C8–C14–C13–C5	0.374	569	−90
43	B_{3g}	1273	38	H17–C3–C4	0.868	1253	20	9	B_{3u}	474	53	C2–C3–C4–C12	0.329	572	−98
42	B_{1u}	1272	41	H20–C6–C7	0.869	1247	25	8	A_g	397	34	C5–C13–C14	2.419	909	−512
41	A_g	1264	36	H15–C1–C2	0.873	1256	8	7	B_{3g}	397	33	C8–C14–C13	2.419	909	−512
40	B_{3g}	1187	15	C4–C12	5.475	1245	−58	6	B_{3u}	380	60	C7–C6–C5–C13	0.329	572	−192
39	B_{2u}	1167	42	H21–C7–C8	0.868	1253	−86	5	B_{2g}	287	54	C3–C4–C12–C11	0.339	564	−277
38	A_g	1164	37	H16–C2–C3	0.869	1247	−83	4	B_{1g}	244	59	C6–C5–C13–C14	0.339	564	−320
37	B_{1u}	1147	12	C1–C11	5.475	1245	−98	3	B_{1u}	234	28	C2–C3–C4	2.179	893	−659
36	B_{2u}	1124	17	C5–C13	5.475	1245	−121	2	A_u	137	63	C1–C11–C9–C14	0.364	380	−243
35	B_{3g}	1102	20	C8–C14	5.475	1245	−143	1	B_{3u}	106	64	C5–C13–C10–C12	0.364	380	−274
34	A_g	1007	18	C6–C7	5.432	1240	−233	ZPE		118.10				123.90	−5.79
33	B_{2u}	998	13	C2–C3	5.432	1240	−242								

[a]For each local mode, the driving internal coordinate and the coupling frequencies ω_{coup} is given. Zero-point energies (ZPE in kcal/mol) are added to verify the ZPE-additivity requirement ZPE(total) = ZPE(local) + ZPE(coup). Bending and torsional force constants are given in mdyn Å/rad^2. For a numbering of atoms, see Figure 1.

where R_{opt} is normally determined from the single and double bond lengths of Kekule benzene as set up by the CC bonds of trans 1,3-butadiene. The empirical constant α is used to fix the index HOMA to zero for Kekule benzene, and N_B is the number of CC bonds in the conjugated cyclic system analyzed. R_i denotes an individual bond length in the molecule under consideration.[40] The HOMA index based on bond lengths has been amply used;[37−40] however, the bond length R is often a problematic bond strength descriptor.[11]

It has been recently shown by Andrzejak and co-workers[55] that HOMA indices calculated via eq 11 strongly depend on (i) the parameter used for the trans-1,3-butadiene and (ii) the model chemistry used for the calculation of the bond lengths R_i of the π-systems under consideration. In addition, one has to consider that an R_{opt} derived from trans-1,3 butadiene leads to a HOMA index for benzene, the aromatic molecule per se, which is smaller than 1.

To avoid these problems, we base HOMA indices on the local stretching force constants and RBSO values derived from experimental frequencies. Furthermore, we consider benzene as the reference system with optimal bond lengths, as in this way its aromatic delocalization index can be set to 1.00 in the case of **1**.

However, we also define the Kekule benzene via the vibrational frequencies of trans-1,3-butadiene[21] and the corresponding RBSO values. Hence, the modified HOMA leads to an aromatic delocalization index AI, which uses the experimentally based RBSO values n according to

$$AI = 1 - \frac{\gamma}{N_B} \sum (n_{opt} - n_i)^2 \tag{12}$$

with $n_{opt} = 1.468$ for benzene. The parameter $\gamma = 7.256$ is determined via the condition that the HOMA index for the Kekule benzene is 0, in line with the original literature.[37−40] Equation 12 can be reformulated to

$$AI = 1 - \gamma \left[(n_{opt} - n_{av})^2 + \frac{1}{N_B} \sum (n_{av} - n_i)^2 \right]$$
$$= 1 + WS + ALT \tag{13}$$

Here, n_{av} is an averaged bond order, WS gives the weakening (strengthening) of bonds compared to the average bond strength (reflected by n_{av}), and ALT reflects the degree of bond strength alternation.

Table 2. Experimental Normal Mode Frequencies ω_μ and the Corresponding Local Mode Force Constants k_n^a and Frequencies ω_n^a of Phenanthrene (4)^a

μ	sym.	ω_μ [cm^{-1}]	#	param.	k^a [mdyn Å^{-1}]^a	ω^a [cm^{-1}]	ω_{coup} [cm^{-1}]
66	A_1	3094	4	C4–H18	5.174	3073.4	20.6
65	B_2	3082	5	C5–H19	5.174	3073.4	8.6
64	A_1	3072	2	C2–H16	5.099	3051.0	21.0
63	B_2	3064	7	C7–H21	5.099	3051.0	13.0
62	A_1	3057	9	C9–H23	5.045	3034.9	22.1
61	B_2	3047	6	C6–H20	5.092	3048.8	-1.8
60	A_1	3037	3	C3–H17	5.092	3048.8	-11.8
59	B_2	3024	1	C1–H15	5.004	3022.4	1.6
58	B_2	3019	10	C10–H24	5.045	3034.9	-15.9
57	A_1	3002	8	C8–H22	5.004	3022.4	-20.4
56	A_1	1626	22	C9–C10	7.755	1481.1	144.9
55	B_2	1616	19	C7–C8	6.790	1386.0	230.0
54	A_1	1602	11	C1–C2	6.790	1386.0	216.0
53	B_2	1572	13	C3–C4	6.704	1377.1	194.9
52	A_1	1526	17	C5–C6	6.704	1377.1	148.9
51	B_2	1502	12	C2–C3	5.900	1291.9	210.1
50	B_2	1458	30	H18–C4–C12	0.925	1285.3	172.7
49	A_1	1443	18	C6–C7	5.900	1291.9	151.1
48	A_1	1431	31	H19–C5–C13	0.925	1285.3	145.7
47	B_2	1424	20	C8–C14	5.784	1279.1	144.9
46	A_1	1352	34	H22–C8–C14	0.922	1279.4	72.6
45	B_2	1340	27	H15–C1–C2	0.914	1279.0	61.0
44	A_1	1304	25	C11–C1	5.784	1279.1	24.9
43	B_2	1282	35	H23–C9–C14	0.916	1273.0	9.0
42	A_1	1247	36	H24–C10–C11	0.916	1273.0	-26.0
41	B_2	1227	29	H17–C3–C2	0.905	1270.2	-43.2
40	A_1	1203	32	H20–C6–C7	0.905	1270.2	-67.2
39	B_2	1173	14	C4–C12	5.692	1268.9	-95.9
38	A_1	1163	16	C5–C13	5.692	1268.9	-105.9
37	A_2	1159	55	H15–C1–C2-H16	0.215	1023.7	135.3
36	B_1	1149	60	H21–C7–C8-H22	0.215	1023.7	125.3
35	A_1	1144	28	H16–C2–C3	0.896	1264.5	-120.5
34	B_2	1144	24	C13–C14	5.530	1250.8	-106.8
33	A_1	1094	33	H21–C7–C6	0.896	1264.5	-170.5
32	B_2	1040	23	C10–C11	5.412	1237.3	-197.3
31	A_1	1038	26	C11–C12	5.530	1250.8	-212.8
30	B_2	1001	21	C9–C14	5.412	1237.3	-236.3
29	A_2	969	56	H16–C2–C3–H17	0.202	986.5	-17.5
28	B_1	950	59	H20–C6–C7–H21	0.202	986.5	-36.5
27	A_2	946	57	H17–C3–C4–H18	0.202	977.8	-31.8
26	B_2	876	15	C13–C12	4.997	1189.0	-313.0
25	B_1	871	58	H19–C5–C6–H20	0.202	977.8	-106.8
24	A_1	832	43	C8–C14–C13	2.597	952.8	-120.8
23	B_1	817	61	H23–C9–C14–C8	0.216	774.6	42.4
22	A_2	791	62	H24–C10–C11–C1	0.216	774.6	16.4
21	A_2	763	64	H18–C4–C12–C13	0.187	740.3	22.7
20	A_2	761	47	C1–C2–C3–C4	0.341	576.2	184.8
19	B_1	732	63	H19–C5–C13–C12	0.187	740.3	-8.3
18	B_1	715	48	C2–C3–C4–C12	0.324	570.5	144.5
17	B_2	712	44	C14–C13–C5	2.673	961.3	-249.3
16	A_1	711	42	C11–C12–C13	2.594	936.6	-225.6
15	B_2	619	45	C13–C5–C6	2.393	934.2	-315.2
14	A_2	594	46	C11–C1–C2–C3	0.337	574.7	19.3
13	A_1	548	41	C10–C11–C12	2.481	924.8	-376.8
12	A_2	546	49	C9–C10–C11–C12	0.322	558.4	-12.4
11	B_2	536	37	C11–C1–C2	2.381	931.8	-395.8
10	B_1	495	54	C13–C5–C6–C7	0.324	570.5	-75.5
9	B_2	441	40	C9–C10–C11	2.307	918.2	-477.2
8	B_1	426	53	C14–C13–C5–C6	0.315	544.0	-118.0
7	A_1	408	38	C1–C2–C3	2.313	916.4	-508.4
6	A_2	395	52	C8–C14–C13–C5	0.327	538.5	-143.5
5	A_1	247	39	C2–C3–C4	2.305	916.4	-669.4
4	A_2	246	51	C11–C12–C13–C14	0.248	465.5	-219.5
3	B_1	234	50	C10–C11–C12–C13	0.298	514.4	-280.4
2	B_1	124	65	C8–C14–C13–C12	0.399	379.9	-255.9
1	A_2	97	66	C1–C11–C12–C13	0.399	379.9	-282.9
ZPE		118.88				124.56	-5.67

^{a}For each local mode, the driving internal coordinate and the coupling frequencies ω_{coup} is given. Zero-point energies (ZPE in kcal/mol) are added to verify the ZPE-additivity requirement ZPE(total) = ZPE(local) + ZPE(coup). Bending and torsional force constants are given in mdyn Å/rad². For numbering of atoms, see Figure 1.

The normal vibrational modes can be characterized in terms of local vibrational modes using the CNM (characterizing normal modes) approach by Konkoli and Cremer[56] as integrated in the quantum chemical program package COLOGNE2013.[57] In this work, the results of the CNM analysis are given in form of bar diagrams, which give the contributions of the various local modes to a specific normal mode (in %) in the form of color coded ranges of a bar.

■ RESULTS AND DISCUSSION: VIBRATIONAL FREQUENCIES AND RBSO VALUES

The four aromatic molecules 1−4 investigated in this work are shown in Figure 1 where all atoms are numbered and bonds are given special symbols (α-,β-, etc.; i: inner; c: central; b: bridge; d: double bond) for quick identification. In Table 1 and Table 2, the experimental frequencies of anthracene and phenanthrene are listed.[23−29] For each normal-mode frequency ω_μ, the corresponding local mode force constants k_n^a and frequency ω_n^a, the parameter, which drives the local mode (given according to the notation in Figure 1), and the coupling frequency ω_{coup}, which gives a measure of mode−mode coupling, are listed. The zero point energy is calculated

for the normal-mode frequencies and expressed in the form of the two contributions: ZPE(normal) = ZPE(local) + ZPE(coup).

In Figure 2 and Figure 3, the ACSs of anthracene and phenanthrene based on the experimental frequencies[23−29] are shown. For anthracene ($3N − 6 = 66$), 10 CH bond lengths, 16 CC bond lengths, 9 CCC, and 10 HCC bond angles as well as 6 HCCH, 4 HCCC, and 11 CCCC bond dihedral angles were derived from a redundant parameter set as leading parameters for the 66 local vibrational modes in the ACS. For phenanthrene, a similar set was derived with the help of the ACS diagram.

Anthracene has a heat-of-formation $\Delta H_0^f(298) = 55.0 \pm 0.7$ kcal/mol, and by this it is 6.8 kcal/mol less stable than phenanthrene ($\Delta H_0^f(298) = 48.2 \pm 0.7$ kcal/mol).[58−60] The ZPE values in Table 1 and Table 2 (118.10 and 118.88 kcal/mol) reveal that the electronic energy difference should be at least 0.8 kcal/mol larger (i.e., 7.6 kcal/mol) because the ZPE favors the stability of anthracene. For both molecules, local and coupling contributions reproduce the ZPE values: 123.90 − 5.80 = 118.10 kcal/mol (Table 1) and 124.59 − 5.71 = 118.88 kcal/mol (see Table 2).
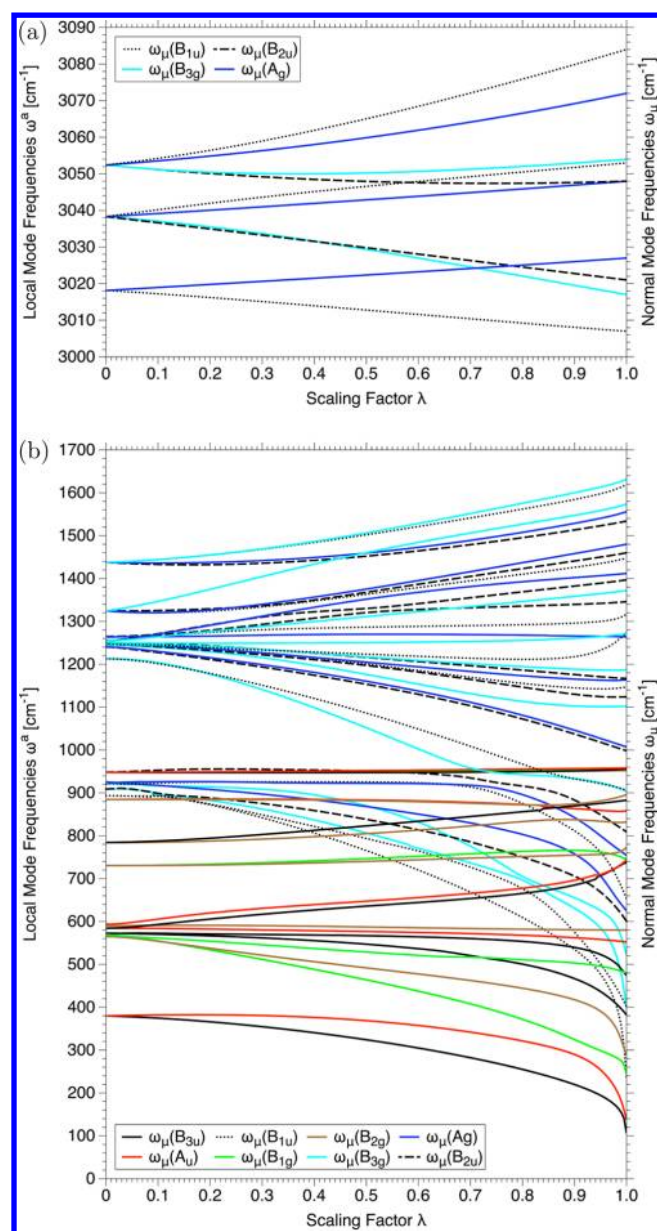
Figure 2. Adiabatic connection scheme (ACS) of anthracene (**3**) based on experimental frequencies. Panels a and b show the upper and lower frequency ranges, respectively. For details, see Table 1.

Figure 3. Adiabatic connection scheme (ACS) of phenanthrene (**4**) based on experimental frequencies. Panels a and b show the upper and lower frequency ranges, respectively. For details, see Table 2.

In the following, the vibrational properties of **3** and **4** are discussed. Those of **1** and **2** are summarized in the tables and figures of the Supporting Information (see also ref 32).

The Vibrational Properties of Anthracene (3). The local mode frequencies of **3** listed in Table 1 and shown in the ACS diagrams in Figure 2a,b provide an easy understanding of the ordering and the character of the normal-mode frequencies. Local CH stretching frequencies are found in the range 3018−3052 cm^{-1} and, because of mode−mode coupling extend to the range 3007−3084 cm^{-1}. The lowest CH stretching frequencies are found for the *i*-CH bond (C9H23 and C10H24, Figure 1) stretchings, whereas the highest values result from the four *β*-CH bond (C2H16, C3H17, C6H20, and C7H21) stretchings. The local stretching frequencies of the *α* CH-bonds (C1H15, C4H18, C5H19, and C8H22) at 3038 cm^{-1} take a middle position in the ACS (see Figure 2a).

The close packing of the local CH stretching frequencies in a range of just 34 cm^{-1} leads, upon mode−mode coupling and the
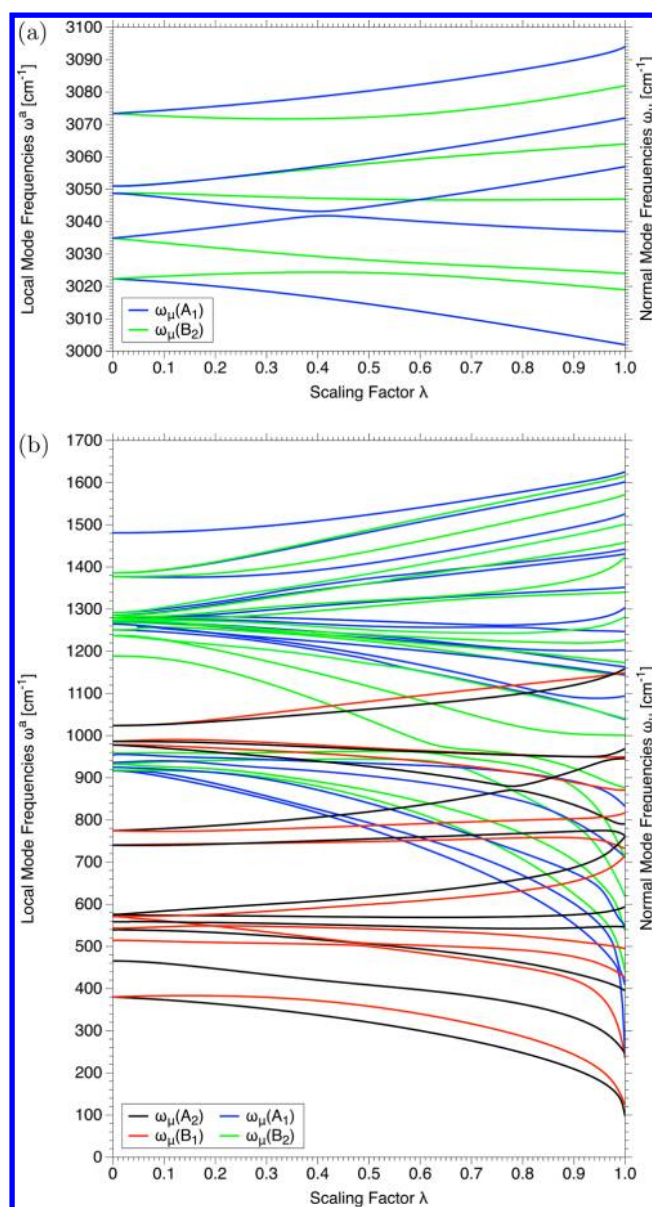
resulting splitting of equivalent CH stretching frequencies into symmetric (A_g) and antisymmetric (*B*-type) combinations, to allowed crossings between eigenstates of different origin (*β* and *α*; *α* and *i*; see Figure 2a). The latter depend on the closeness of the local frequencies of different groups, the degree of degeneracy, the similarity in masses, the geometrical closeness of vibrating centers, and the orientation of the mode vectors. If the latter are parallel, a maximal, and for perpendicular orientation, a minimal coupling effect results. For example, the *i*-CH stretching couples with the two neighboring *α*-CH stretchings (the mode vectors are parallel and the frequencies are just 20 cm^{-1} apart), but the resulting splitting is also just 20 cm^{-1} (Figure 2a, Table 1) because of the 2-bond separations between the three corresponding mode vectors. The decomposition of the normal modes is given in the Supporting Information and gives quantitative data for mode−mode mixing.

The coupling frequencies of all CH stretchings are smaller than 32 cm^{-1}, which is a direct reflection of the fact that in all

cases the CH bonds are separated by at least one CC bond and, if the latter is the case, the mode vectors form angles of about 60°. Nevertheless, the correct assignment of the measured mode frequencies to specific CH stretchings is because of mode coupling and eigenstate crossing difficult without the local stretching frequencies of Table 1 and the ACS diagram in Figure 1. Noteworthy is that the peri-effect (exchange repulsion between i- and α-H atoms) leads to a lowering of the frequencies of both i- and α-CH stretchings, where, because of their central position, the i-CH bonds have the lowest local stretching frequencies.

The correct assignment of normal-mode frequencies to specific structural units becomes even more difficult for the CC stretching frequencies, which spread over the ranges 1213–1438 cm^{-1} (local modes) and 903–1632 cm^{-1} (normal modes), respectively, i.e., due to mode mixing the range extends by a factor of 3.2. The coupling takes place between CC stretching modes themselves and also involves CCC and HCC bending modes. The lowest local CC stretching frequency (923 cm^{-1}) is found for the c-bonds, whereas the largest frequencies (1438 cm^{-1}) are observed for the β-CC bonds. This is also found for **2** (see Supporting Information).

Local HCC bendings are observed in a relatively small range from 1247 to 1265 cm^{-1}, which due to coupling extends to 1102 to 1412 cm^{-1}. Small ranges are also found for the HCCH (local: 885–948 cm^{-1}; normal: 858–958 cm^{-1}) and HCCC torsional modes (local: 730–784 cm^{-1}; normal: 747–883 cm^{-1}). Frequency ranges for CCC bendings (local: 893–948 cm^{-1}; normal: 243–809 cm^{-1}) and CCCC torsions (local: 380–595 cm^{-1}; normal: 106–743 cm^{-1}), although still small for the local frequencies, are much larger for the normal frequencies.

The Vibrational Properties of Phenanthrene (4). The CH stretching frequencies stretch now over a somewhat larger range (local: 3022–3073 cm^{-1}; normal: 3002–3094 cm^{-1}) of 49 and 92 cm^{-1}, respectively. The local frequencies arrange in 5 pairs where the δ-CH stretching frequencies (in the bay of **4**) are the highest (3073 cm^{-1}), followed by the β- and γ-CH stretching frequencies (3052 and 3050 cm^{-1}), and finally the α- and i-frequencies at 3035 and 3023 cm^{-1}. The peri-effect is again responsible for the low values of the latter. Different from the anthracene spectrum, the splitting of the CH-frequencies, caused by mode–mode coupling, leads to avoided crossings between modes of the same symmetry. At the avoided crossings, the mode character is largely exchanged between the modes, which implies another complication for the assignment of measured normal-mode frequencies to structural units. In Table 2, all avoided crossings and the corresponding changes in the mode character are accounted for correctly.

As in the case of anthracene, the CC stretching frequencies are found in a larger range because of strong mode–mode coupling (local: 1189–1481; normal: 876–1626 cm^{-1}), where each CC bond can be assigned to a specific stretching frequency (see below). For the bending (CCH: 1264–1299 and 1040–1502; CCC: 916–952 and 247–832 cm^{-1}) and torsional modes (HCCH: 978–1024 and 871–1159; HCCC: 740–775 and 732–817; CCCC: 380–576 and 97–761 cm^{-1}), the ranges of observed frequencies differ somewhat from those found for anthracene; however, in each case the deviations can be explained using the local force constants and relating them to the topology and electronic structure of **4** (see below).

Variations in the CH Bond Strength. The RBSO values for the CH bonds are plotted in dependence of the local CH stretching force constants in Figure 4b. There is only a small variation in the RSBO values n of the CH bonds where those in
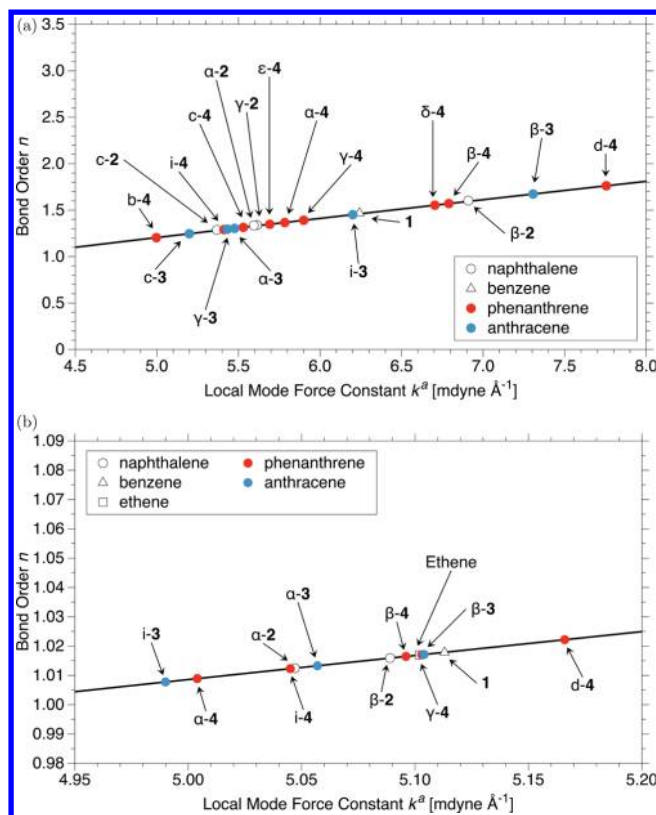

Figure 4. Relative bond strength orders (RBSO) n of CC and CH as a function of their local stretching force constants k^a. (a) RBSO values for CC bonds: $n = 0.29909(k^a)^{0.86585}$. (b) RBSO values for CH bonds: $n = 0.52136(k^a)^{0.40999}$.

benzene are found to be the strongest ($n = 1.010$) of all aromatic CH bonds investigated in this work. This indicates that the benzene ring presents an ideal situation of aromatic π-delocalization. Only the δ-CH (C4H18 and C5H19) bonds in **4** are significantly stronger, which has to be explained in this work.

The strength of the CH bonds is reduced in the case of peri-interactions because of increased exchange repulsion between the electron pairs of i- and α-CH bonds (or α-CH bonds in the case of **2**). Since the i-CH bonds in **3** experience two of these interactions, they are the weakest of all CH bonds in the four aromatic ring systems. The α-CH bonds (C1H15, C8H22) in phenanthrene are somewhat stronger; however, they are also weakened by peri-repulsion as are the neighboring i-bonds (C9H23 and C10H24) in the same molecule (see Table 3 and Figure 4b). Next in line are the peri-CH bonds in naphthalene and anthracene.

Based on these results, one has to conclude that the CH bond strength in the aromatic ring systems investigated is primarily influenced by peri-repulsion of (almost) parallel oriented bonds, whereas the change in sp^2-hybridization caused by different delocalization situations in the four-ring systems represents only a second order effect, which nevertheless is reflected by the CH local mode properties and the RBSO values based on them. Considering just the β (and γ)-CH bonds, the following RBSO order is obtained: benzene > anthracene > phenanthrene > naphthalene, all of them being close to the RBSO value of ethene. It remains to be discussed how this order of the CH bond strength relates to the π-delocalization in the various benzoid systems.

Table 3. CH and CC Bond Lengths, Experimentally Based Local Mode Force Constants, RBSO Values n, Electron Density ρ_c, Energy Densities V_c, G_c, and H_c at the Path Critical Points r_c.[a]

mol.	bond	r [Å]	k_n^a [mdyn Å^{-1}]	n	ρ_c [e Å^{-3}]	V_c [h Å^{-3}]	G_c [h Å^{-3}]	H_c [h Å^{-3}]
1	C1−H7	1.086	5.113	1.010	1.917	−2.288	0.283	−1.998
2	C1−H11	1.087	5.047	1.007	1.910	−2.274	0.290	−1.991
2	C2−H12	1.086	5.089	1.009	1.917	−2.288	0.283	−2.004
3	C1−H15	1.083	5.057	1.013	1.930	−2.321	0.297	−2.031
3	C2−H16	1.082	5.104	1.017	1.937	−2.335	0.290	−2.038
3	C9−H23	1.084	4.990	1.008	1.923	−2.315	0.297	−2.018
4	C1−H15	1.087	5.004	1.009	1.910	−2.281	0.290	−1.991
4	C2−H16	1.086	5.103	1.017	1.917	−2.288	0.283	−2.004
4	C3−H17	1.086	5.096	1.016	1.917	−2.288	0.283	−2.004
4	C4−H18	1.084	5.166	1.022	1.930	−2.315	0.297	−2.018
4	C9−H23	1.087	5.045	1.012	1.917	−2.281	0.290	−1.991
5	C1−H3	1.095	4.787	0.991	1.863	−2.213	0.310	−1.896
6	C1−H4	1.087	5.102	1.017	1.910	−2.274	0.283	−1.991
7	C1−H3	1.066	5.905	1.080	1.964	−2.423	0.250	−2.173
8	C1−H2	1.092	4.897	1.000	1.863	−2.213	0.310	−1.903
1	C1−C2	1.396	6.242	1.468	2.105	−2.774	0.668	−2.105
2	C1−C2	1.376	6.909	1.603	2.180	−2.996	0.742	−2.261
2	C1−C9	1.421	5.595	1.335	2.018	−2.517	0.587	−1.930
2	C2−C3	1.417	5.614	1.339	2.031	−2.558	0.601	−1.950
2	C9−C10	1.434	5.368	1.288	1.984	−2.423	0.567	−1.856
3	C1−C11	1.425	5.476	1.304	2.004	−2.470	0.574	−1.896
3	C1−C2	1.363	7.306	1.673	2.234	−3.158	0.783	−2.375
3	C11−C12	1.440	5.199	1.246	1.964	−2.362	0.547	−1.815
3	C2−C3	1.421	5.432	1.295	2.011	−2.504	0.580	−1.923
3	C9−C11	1.395	6.201	1.452	2.119	−2.780	0.668	−2.112
4	C1−C11	1.414	5.784	1.367	2.045	−2.585	0.614	−1.971
4	C1−C2	1.380	6.790	1.571	2.166	−2.949	0.722	−2.227
4	C11−C12	1.427	5.530	1.315	2.004	−2.483	0.594	−1.890
4	C12−C13	1.458	4.997	1.204	1.890	−2.186	0.499	−1.680
4	C2−C3	1.407	5.900	1.391	2.065	−2.652	0.628	−2.025
4	C3−C4	1.383	6.704	1.553	2.153	−2.922	0.715	−2.207
4	C4−C12	1.415	5.692	1.348	2.038	−2.578	0.614	−1.964
4	C9−C10	1.359	7.755	1.762	2.247	−3.212	0.803	−2.409
4	C9−C14	1.435	5.412	1.291	1.971	−2.382	0.547	−1.836
5	C1−C2	1.531	4.031	1.000	1.640	−1.674	0.364	−1.302
6	C1−C2	1.330	8.976	2.000	2.342	−3.583	0.931	−2.652
7	C1−C2	1.205	15.820	3.267	2.713	−5.810	1.930	−3.880
1	H7···H8	2.483			0.209	−0.209	0.229	0.020
2	H11···H12	2.471			0.216	−0.223	0.236	0.020
2	H11···H18	2.484			0.047	−0.027	0.040	0.013
2	H12···H13	2.491			0.202	−0.196	0.223	0.020
3	H15···H16	2.456			0.223	−0.229	0.250	0.020
3	H15···H23	2.470			0.047	−0.027	0.040	0.013
3	H16···H17	2.483			0.202	−0.196	0.223	0.020
4	H15···H16	2.478			0.216	−0.216	0.236	0.020
4	H15···H24	2.428			0.047	−0.027	0.040	0.013
4	H16···H17	2.494			0.209	−0.202	0.229	0.020
4	H17···H18	2.440			0.209	−0.209	0.229	0.020
4	H18···H19	2.014			0.081	−0.047	0.067	0.020
4	H23···H24	2.464			0.223	−0.229	0.250	0.020
9	H1−H2	0.743	5.706	1.000	1.809	−2.267	0.000	−2.267
10	H1−H2	1.094	1.588	0.500	0.574	−0.391	0.000	−0.391

[a]$H_c = V_c + G_c$ is the energy density at the path-critical point r_c, where V_c and G_c denote the potential and kinetic energy density. Energies in h = hartrees. For a numbering of atoms and molecules (Mol), see Figure 1.

■ STRENGTH OF THE CC BONDS AND AROMATICITY

The topology of the ring annelation has a well-defined impact on the strength of the individual CC bonds. Three types of CC bonds can be distinguished: (i) Weakened CC bonds that have a significantly smaller RBSO values (≤1.3) than those of benzene (1.468, Table 3); (ii) typical aromatic CC bonds similar to those in benzene (1.3−1.6); (iii) CC bonds with distinct double bond character (>1.6).
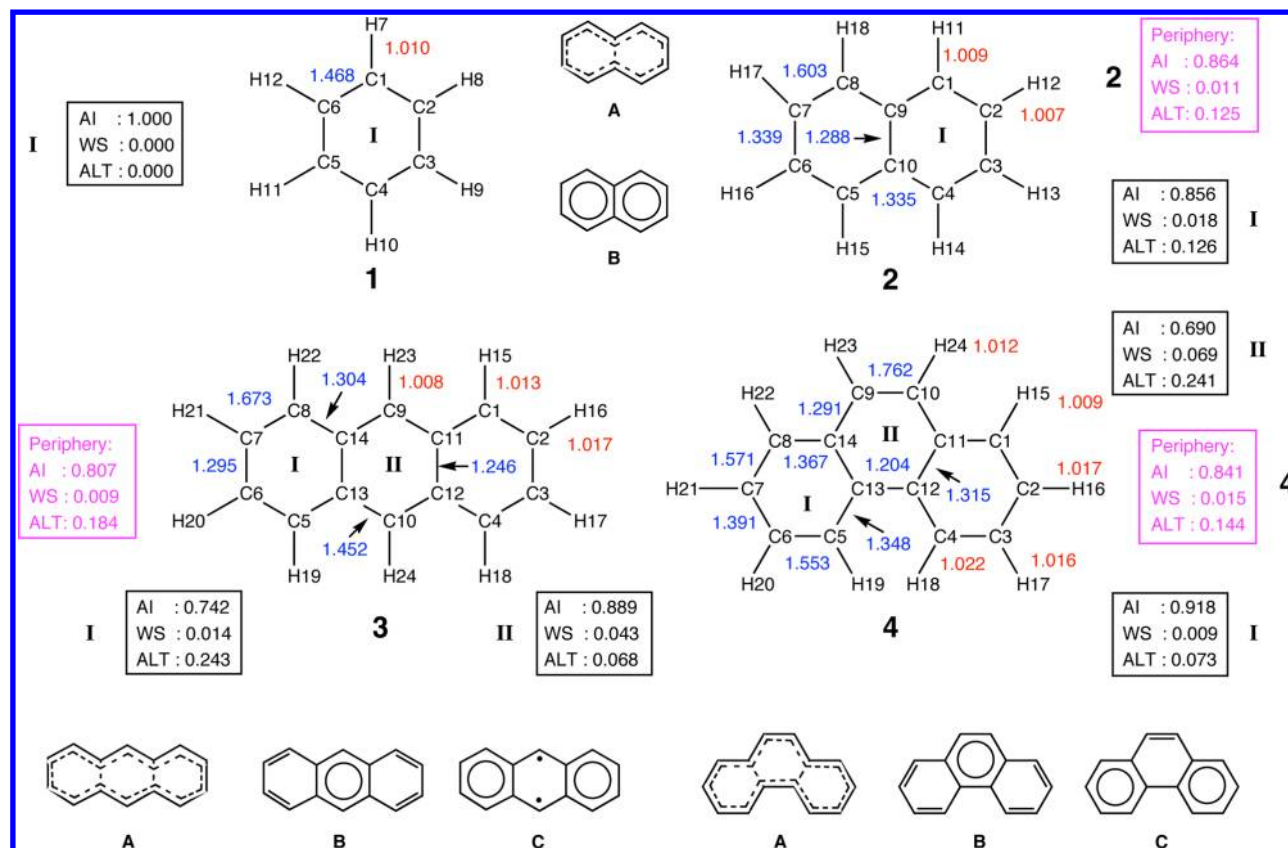
Figure 5. Relative bond strength orders (RBSO, blue: CC; orange CH), delocalization indices AI with WS and ALT parameters (all based on experimental frequencies) given for benzene (**1**), naphthalene (**2**), anthracene (**3**), and phenanthrene (**4**). Delocalization in outer rings **I** and inner rings **II** as well as the peripheral delocalization are given separately. Possible delocalization modes A, B, and C are given for **2**, **3**, and **4** at the bottom.

According to the RBSO values directly derived from experimental frequencies, the weakest CC bonds in molecules **1−4** are the *b*-bond in phenanthrene (C12C13: 1.204), the *c*-bonds in anthracene (C11C12 and C13C14: 1.246) and that in naphthalene (C9C10: 1.288). Only, the *c*-bonds C11C12 and C13C14 (*n* = 1.315) in phenanthrene do not belong to this type. This reflects important features of π-delocalization caused by the topology of ring annelation.

Naphthalene prefers to be a peripherally delocalized 10π-system with a central 9−10 perturbation rather than a system with two benzene rings where the latter compete for the π-electrons of C9 and C10 (see Figure 5). The AI values of 0.864 (periphery) and 0.856 (ring I) suggest this interpretation where the difference is predominantly caused by the central bond (WS(periphery) = 0.011 vs WS(ring I) = 0.018; see Figure 5). Although this effect is relatively small, it corrects an interpretation given by the experimentally determined geometry of **2**: all measured values for the *c*−CC bond (1.420−1.424 Å) are shorter than those for the α-CC bonds (1.422−1.425 Å[61−64]), thus suggesting that the preferred delocalization mode is B in Figure 5, whereas the RBSO values based on the experimental frequencies prefer delocalization mode A. The loss in aromaticity for **2** from 1 down to 0.86 is predominantly caused by an increase in bond alternation due to the C9C10 perturbation (ALT = 0.125), i.e., each ring in **2** has only 86% of the aromaticity of benzene.

With the annelation of a third benzene ring in anthracene, three different π-delocalization modes can be anticipated (see Figure 5). Option A corresponds to the peripheral delocalization of a 14π-system with two central perturbations, option B to a central benzene ring that is annelated at both sides by six-membered rings with distinct butadiene units, and option C to benzene rings connected by a six-membered ring with significant biradical character (positions C9 and C10). Clearly, option C is the least likely because of the destabilization caused by its biradical character. It is difficult to predict whether option A or B describes the preferred delocalization mode of anthracene better.

The AI values for A is 0.807, and the average value for B is 0.791 (averaged over the AI values of the individual rings, eq 11), which suggests that option A is again slightly preferred. In both cases, the aromatic character is decreased to about 80%. In line with option B, the central ring (ring II) has a larger degree of π-delocalization (AI = 0.889) than the two outer ones (ring I: AI = 0.742, Figure 5). Despite the weakening of the *c*-CC bonds C11C12 and C13C14, ring II experiences a relatively modest loss of aromatic character from both bond weakening (WS = 0.043) and bond alternation (ALT = 0.068), whereas for ring I it is predominantly bond alternation (ALT = 0.243), which leads to the strong reduction of aromaticity.

For phenanthrene, the peripheral delocalization with two perturbations (C11C12 and C13C14) has a higher AI value (0.841) than that for anthracene (0.807). However, it is not the best delocalization option. Possibility B is the least favorable in view of an AI of 0.690 for ring II. Option C describes more realistically π-delocalization in phenanthrene: A biphenyl unit (each benzene ring has an AI of 0.918 and therefore comes closest to the ideal case of benzene) is kept in a planar form by the C9C10 bridge, which has a high double bond character with an RBSO of 1.762, i.e., it is the strongest type iii-bond found for **1−4**. The connecting *i*-bonds C10C11 and C9C14 have a much smaller RBSO value of 1.291, which is even smaller than that of

the *c*-bonds C11C12 and C13C14 (1.315). Again this confirms a π-delocalization according to option C.

One might consider the direct use of the RBSO values in an incremental way to determine the heats-of-formation of a benzoid aromatic molecule according to

$$\Delta H_0^f(\text{molecule, 298}) = a \sum_i n_i(\text{CH}) + b \sum_j n_j(\text{CC}) \tag{14}$$

where the summation is over all CH bonds *i* and CC bonds *j*, respectively, and constants *a* and *b* provide the conversion from RBSO values *n* into bond energies and absorb any vibrational and thermochemical corrections. Hence, these constants are empirical and are determined by reproducing the ΔH_0^f values of benzene and naphthalene (a = −0.254 and b = 2.424 kcal/mol). By utilizing eq 14, one obtains $\Delta H_0^f(298)$ values of 52.68 and 52.29 kcal/mol for **3** and **4**, respectively, i.e., the first molecule is described too stable (55.0 kcal/mol[58]) and the second (48.2 kcal/mol[59,60]) too unstable. This confirms that the quantum mechanical effects of π-delocalization cannot be described with a classical model based on the assumption that the π-delocalization is the same in the four systems investigated.

Although the AI values based on experimental frequencies and a modified HOMA qualitatively explain the larger stability of phenanthrene compared to anthracene, it is desirable to quantify the effects of the different π-delocalization modes. This requires one to calibrate the relationship between the resonance energy RE and the AI values, which here is assumed to be linear:

$$\text{RE} = d\text{AI} + e \tag{15}$$

Using homodesmotic reactions[65] and experimental heats-of-formation, the RE value for benzene is found to be 21.1 kcal/mol, where *trans*-1,3-butadiene is the available acyclic reference. Roth and co-workers[66,67] pointed out that *cis*- rather than *trans*-1,3-butadiene would be better suited as a reference. By combining experimental and force field data, they obtained a homodesmotic resonance energy of 25.4 kcal/mol for benzene and 40.1 kcal/mol for naphthalene.[66,67] With these values, constants *d* and *e* are found to be 37.153 and −11.753 kcal/mol, respectively. They lead to RE values of 52.9 and 58.6 kcal/mol for **3** and **4**, thus predicting that a difference in the RE values of 5.7 kcal/mol is the major reason for the difference in the experimental $\Delta H_0^f(298)$ values of 55.0 and 48.2 kcal/mol, which turns out to be 6.8 kcal/mol.[59,60]

In summary, the HOMA-RSBO analysis explains that the different topologies of ring annelation in **3** and **4** are responsible for the larger stability of the latter compared to the former. For **4**, possibility C in Figure 5 is the preferred π-delocalization mode, which leads to the dominance of two benzene units in the delocalization pattern, whereas in the case of **3** possibility B dominates, which has only one benzene unit in the center. It remains to be seen whether this conclusion has to be reconsidered in view of different H,H interactions in the two benzoid hydrocarbons (see below).

Interactions between Hydrogen Atoms. As described in Section 2, the ACS was used with a large set of redundant coordinates including H,H-distances to determine a non-redundant set of N_{vib} internal coordinates, which can operate as leading parameters for N_{vib} local vibrational modes. None of the H,H-interactions turned out to drive a local vibrational mode that relates to any of the N_{vib} normal vibrational modes, i.e. in the ACSs of **1−4** local mode frequencies associated with H,H interactions converge to zero for $\lambda \rightarrow 1$. This is also true for the interaction H18,H19 (distance: 2.014 Å) in the bay region of phenanthrene.

Hence, intramolecular H,H interactions cannot be directly investigated via the local vibrational modes, but only indirectly via the CH stretching modes as in the case of the bay hydrogen atoms of phenanthrene. The γ-CH (C4H18 and C5H19) stretching frequencies, their force constants, and the corresponding bond orders (1.022, Table 3, Figure 5) are clearly the largest in phenanthrene and the four aromatic systems investigated. This indicates that, upon CH stretching, the potential energy steeply increases, which in turn confirms that there is exchange repulsion between atoms H18 and H19. Any weak stabilizing interactions, for example due to H,H-dispersion interactions, are outweighed by exchange repulsion so that, in total, no H···H attractive interactions exist.

Comparison with Other Results. Matta and co-workers[41] found for the H18,H19 interaction in phenanthrene a path of maximum electron density (MED), which is the necessary criterion for covalent bonding. These authors concluded erroneously that the existence of such a path implies a stabilizing H,H interaction. Although, these authors did not use the term covalent H,H interaction, their description was understood to indirectly suggest a covalent H,H interaction. Already in the 1980s, Cremer and Kraka[3,68,69] pointed out that the existence of a MED path is only a necessary condition for covalent bonding, which has to be complemented by the sufficient condition that the energy density at the path-critical point $\mathbf{r}_c$, i.e., $H_c = H(\mathbf{r}_c) = V_c + G_c$ is negative, thus indicating stabilizing attractive interactions between the atoms connected by the MED path. A negative H_c value is caused by a negative (stabilizing) potential energy density outweighing the positive (destabilizing) kinetic energy density.[68,69]

The results of the electron and energy density analysis are listed in Table 3. At the path-critical point $\mathbf{r}_c$ between H18 and H19, the electron density is just 0.012 e Å^{-3} and by this just 14% of the value calculated for H$_2$ (0.085 e Å^{-3}, Table 3). The energy density at this point (0.003 hartree Å^{-3}) is positive due to a slight dominance of the kinetic energy density (Table 3). Thus, the energy density is indicative of an electrostatic, repulsive interaction typical of sterically congested CH bonds. Positive energy densities H_c are also found for all other H,H interactions investigated for molecules **1−4**, although in the latter cases, no MED paths connect vicinal H atoms. Therefore ρ_c and H_c were calculated at the midpoint between the H atoms. It is interesting to note that the electron and energy density values at these midpoints often turn out to be larger than the corresponding values at the path-critical point between H18 and H19. In line with the fact that the ACS procedure leads to zero frequencies for all H,H interactions (see Table 3), the existence of a MED path between between the bay-hydrogens of **4** has no energetic relevance.

Since the bay CH bonds of phenanthrene have larger RSBO values, the question remains whether different CH bond strengths change the relative stabilities of **3** and **4**. By simply summing over all RSBO(CH) values of a given molecule, values of 10.136 (**3**) and 10.152 (**4**) are obtained. According to eq 14, this corresponds to a small difference in the energy contributions to ΔH_0^f of less than 0.01 kcal/mol and, therefore, is not relevant. Since the vibrational frequencies sensitively absorb into their values environmental effects, there is no basis to partition contributions into bonded and nonbonded (exchange repulsion) contributions. Furthermore, differences resulting from bending or torsional vibrations are contained in the ZPE difference of 0.8 kcal/mol (in favor of **3**), which in turn is absorbed into the resonance energies used above because these correspond to normal thermodynamic conditions.[66,67]

Hence, the vibrational analysis of bonding in phenanthrene and anthracene clearly confirms the results of π-delocalization

studies, which date back to the 1930s[70] and which all predict molecule **4** being more resonance stabilized than molecule **3**. In the 1970s, Clar[71] pointed out that any system with a larger number of aromatic π-sextets is more stable than that with a lower one. This is in line with the RSBO description suggesting two benzene sextets for **4** (structure C in Figure 5) and just one for **4** (structure B in Figure 5).

Furthermore, the vibrational description is in line with the magnetic properties of the two benzoid aromatic hydrocarbons. Magnetic properties provide a sensitive measure for π-delocalization effects.[4,7,9] Aromatic delocalization is accompanied by a distinct ring current in a cyclic system. Investigations of **3** and **4**[72−76] clearly show that ring currents are localized in the central ring of **3**, whereas they are more significant in the outer rings of **4**. Hence, the magnetic description of π-delocalization is in line with the vibrational description that favors structures B and C of Figure 5.

There is a clear agreement based on all experimental[59,60,77−80] and computational investigations[5,42,45,81−87] that the larger stability of **4** compared to that of **3** is the result of a more effective π-delocalization. Especially, the recent work by Bickelhaupt and co-workers[42] has to be mentioned in this connection who demonstrated the better π-delocalization in **4** via a quantitative energy decomposition analysis utilizing 2-methtriyl-phenyl fragments.

Grimme and co-workers[43] synthesized D18,D19-phenanthrene and measured its Raman and infrared spectrum to obtain information about the H,H interactions in the phenanthrene bay region. They found at room temperature for the solid compound C−D infrared stretching frequencies at 2288 cm^{-1} (A_1) and 2278 cm^{-1} (B_2), i.e., the symmetric is above the antisymmetric combination of the two CD stretching frequencies, and their splitting is 10 cm^{-1} (similar results were obtained by the Raman spectroscopical investigation[43]). Utilizing the experimental frequencies given in Table 2 and the perturbation approach described in Section 2, we obtain 2280 cm^{-1} (A_1) and 2269 cm^{-1} (B_2), leading to a splitting of 11 cm^{-1}, which is in line with the data of Grimme and co-workers considering the different experimental conditions for the measurement of the vibrational spectra of the deuterated **4** and the parent compound and the small errors made by using the perturbation approach described in Section 2.

We note also that the direct analysis of **4** gives a splitting of 12 cm^{-1} (3094 cm^{-1} for A_1-symmetrical mode 66 and 3082 cm^{-1} for the B_1-symmetrical mode 65), where, however, it has to be considered that both modes have admixtures of 11% from other modes. The corresponding admixtures for the CD stretching modes are 4%. Despite the mass effect, the CD stretching modes still do have small couplings with CC stretching and CCC bending modes; however, the effects are for the parent molecule and the deuterated isotopomer are relatively small. This underlines that, by using the approach presented in this investigation, the vibrational spectrum of the parent molecule **4** would have been sufficient to obtain the results of Grimme and co-workers in just a fraction of the time needed to synthesize and investigate deuterated phenanthrene.

The conclusions drawn in the current investigation and in many other investigations is that the H18,H19 interactions in **4** are irrelevant for the stability of phenanthrene. Our investigation reveals in addition that the changes in the CH bond strengths of **3** and **4** cancel each other largely. Interesting is the fact that the H18,H19 interaction leads to a shortening and strengthening of the corresponding CH bonds (RSBO: 1.022 compared to 1.017 for the next strongest bonds in **3** and **4**), which distinguishes

these CH bonds clearly from the i-CH bonds in **3** or the α-CH bonds in **2** and **4**.

The strength of the δ-CH bonds in **4** may be on first sight surprising in view of the expected exchange repulsion between H atoms separated by a distance of just 2.014 Å. This exchange repulsion is, however, different than in the case of the peri-positioned CH bonds in **2** or **3**, which, due to their parallel orientation mutually push electron density out of the CH connection line, thereby weakening the CH bonds. In **4**, the two bay-located CH bonds enclose an angle of about 60°, which leads to the fact that a lowering of the exchange-repulsion can only be achieved by a shortening and, thereby, strengthening of the CH bond. The second bay-CH bond confines the space for the first bay CH bond, increases the potential walls, stiffens the bond, and makes its stronger. Hence, this is a situation where bond strengthening is a result of space confinement.

Bader[44] criticized the work by Grimme and co-workers[43] as not considering the quantum mechanical forces, which lead to a MED path between atoms H18 and H19.[41] He described these forces, but failed to consider some of the arguments he himself had brought up in earlier work:[88]

(i) The interaction between two atoms is not only given by the mere existence of an MED path. The electron density properties of the MED path, especially those at the path-critical point matter as well. In the case of the H18,H19 interaction, the electron density is very small, and the energy density is slightly positive (Table 3). Furthermore, the MED path is curved inwardly toward the center of the bay region. The electron density of the path critical point and the ring critical point are almost identical (difference <0.003 electron Å^{-3}).[41] Hence, a situation exists in which the path and ring critical points are close enough to merge and the MED path between atoms H18,H19 ceases to exist.[3] In other words, the existence of a H18−H19 MED path, although quantum mechanically interesting, cannot have a significant impact on the stability of **4** and may be even questionable as long as high-accuracy, vibrationally averaged densities are missing.

(ii) The interaction between two atoms is reflected by the density distribution in the zero-flux surface separating their virial basins.[88] A depletion of electron density caused by exchange repulsion can only be seen when integrating over the zero-flux surface and relating the integrated density value to a suitable reference.[89] A single-point analysis, even if carried out at the path-critical point, does not provide a description of exchange interactions. Hence, the existence of a MED path does not exclude destabilizing exchange interactions.

(iii) Chemistry develops its concepts and models often by using suitable reference values. Explicit references are used, when discussing molecular energies and implicit references when considering the atomic charges of a molecule. Confusion results when the absolute charges and energies of the virial basins are compared with the corresponding referenced quantities, which chemists are using.[3]

The measured ^5J NMR spin−spin coupling constant of 0.55 Hz[59] for the proton,proton interaction H18,H19 is typical for a long-range through-bond coupling mechanism and does not indicate any through-space contributions. Also, the strain energy of **4** was determined to be 1.2 kcal/mol. Since most of this strain energy should result from the steric repulsion between H18,H19, the latter cannot be large, probably because of CH shortening and an angle of 60° enclosed by the CH bond vectors. Thermodynamics, vibrational spectroscopy, and NMR spectroscopy all describe the H18,H19 as energetically of minor significance for the stability of **4**. In conclusion, Bader's critique[44]

of the work by Grimme and co-workers[43] fails to describe the consequences of H,H interactions and to explain why **4** is more stable than **3**.

Finally, there is the question of whether local stretching force constants k^a represent better bond strength descriptors than bond lengths r. To clarify this question, in Figure 6 RBSO values n are compared with calculated (B3LYP/aug-cc-pVTZ)
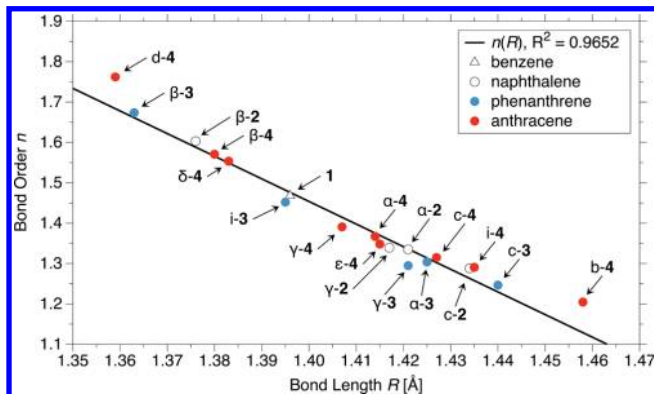

Figure 6. Relative CC bond strength orders n are compared with bond lengths R. Standard deviation σ: 0.028; Kendall τ parameter: -0.917.

CC-bond lengths. Although a linear relationship between these quantities seems to exist, there is also obviously a strong scattering of data points, which reflects the known unreliability of bond lengths as bond strength descriptors.[11] This is confirmed by a standard deviation σ of 0.028 and a Kendall τ parameter of -0.917, which both do not indicate a significant correlation between n and r. Since the bond length is sensitive to the covalent radius of an atom and this can change for an atom because of π-delocalization, charge polarization, and/or bond polarity, the scattering of data points is not surprising in the case of molecules **1**−**4**. The RBSO values based on experimental frequencies reflect fine differences in the CC bond strength, which are not necessarily described by measured or calculated bond lengths.

■ **CONCLUSIONS**

In this work, we have demonstrated how, with a complete set of vibrational frequencies, bond strength descriptors in the form of RBSO values can be derived. For this purpose, a simple perturbation approach is used that leads from measured vibrational frequencies to the corresponding force constant matrix utilizing the normal mode vectors from a reliable quantum chemical investigation. These vibrational mode properties are sufficient to derive the corresponding local mode properties. The local vibrational modes used are the unique complements of the delocalized normal vibrational modes. The local stretching force constants are suitable descriptors of bond strength and are used in this work to describe the CH and CC bonds of benzene and the benzoid molecules **2**, **3**, and **4**. For this purpose, suitable reference bonds have been used, which lead to relative bond strength order (RBSO) values. The following conclusions can be drawn:

(1) The vibrational modes of **3** and **4** can be directly described according to their character. The two highest frequencies of **4** correspond the δ-CH stretching frequencies with the A_1-symmetrical mode at 3094 cm^{-1} being above the B_2-symmetrical mode at 3082 cm^{-1} (splitting of 12 cm^{-1}) and being separated from the other normal CH stretching frequencies. The local δ-CH stretching frequency and force constant identify the δ-bonds

as the strongest CH bonds in **1**−**4**. This is a result of exchange repulsion leading to a shortening and increased polarity of the δ-bonds.

(2) For the D18,D19-phenanthrene, we obtain, by using a perturbation approach, 2280 cm^{-1} (A_1) and 2269 cm^{-1} (B_2) leading to a splitting of 11 cm^{-1}, which is in good agreement with the C−D infrared stretching frequencies at 2288 cm^{-1} (A_1) and 2278 cm^{-1} (B_2) (splitting 10 cm^{-1}) measured by Grimme and co-workers.[43]

(3) The local mode frequencies and force constants describe peri-CH bonds as being weakened due to exchange repulsion, whereas exchange repulsion in the case of the δ-bonds of **4** leads to bond strengthening. However, this is not a contradiction because the topology of the bay region of **4** leads to space confinement and a stronger curvature of the PES in the direction of the CH internal coordinate.

(4) The electron density at or close to the path-critical point between H18 and H19 reveals that the MED path is curved inwardly toward the center of the bay, that path-critical and ring-critical points are close to each other, they have about the same very small density value, and that a situation close to a singularity of the density distribution typical of the annihilation of the H,H MED path exists. Hence, the density distribution between H18 and H19 does not affect the stability of **4** in any significant way. Especially, the inward bending of the MED path does not exclude density depletion in the zero-flux surface between H18 and H19 because of exchange repulsion. At the path-critical point, the energy density H_c is positive, in line with an electrostatic, destabilizing interaction between H18 and H19.

(5) A new aromatic delocalization index AI has been derived in this work, which is based on the RBSO values of the CC bonds and HOMA using **1** and Kekule-benzene as suitable references. The advantage of this approach is that measured vibrational frequencies can be converted into stretching force constants and, therefore, provide a sensitive measure of the curvature of the PES of a target molecule at its minimum in the direction of a preselected internal coordinate. Contrary to experimental bond lengths, which are difficult to convert into r_e-bond lengths for larger molecules, measured frequencies are nowadays available for medium-seized molecules with high accuracy. Their transformation into local mode frequencies and force constants, which in turn lead to RBSO values leads directly to AI values using the approach shown in this work.

(6) AI values describe **2**, **3**, and **4** as π-systems with a slight preference for a peripheral 10π- or 10π-delocalization. The second preferred delocalization mode is given by B (central benzene ring with 2 annelated outer rings with distinct bond alternation) in the case of **3** and C (bridged biphenyl structure) in the case of **4** as shown in Figure 5. The larger stability of **4** compared to **3** results almost exclusively from the fact that two rather than just 1 aromatic sextet are established, which is also reflected by the much higher AI values for **4**. The latter are decided by the topology of ring annelation and the resulting c-bond perturbations.

(7) The difference in the heats-of-formation of **3** (55.0 kcal/mol) and **4** (48.2 kcal/mol[59,60]) is 6.8 kcal/mol, which can be reproduced by 5.7 kcal/mol using the resonance energies of Roth and co-workers[66,67] and the AI values obtained from the measured vibrational frequencies. A bond increment approach based on the RBSO values cannot describe the larger stability of **4**, which is a result of the fact that π-delocalization is a quantum mechanical phenomenon.

This work has shown that vibrational spectroscopy provides excellent tools to describe the electronic structure and chemical bonds. There are not many molecular properties that can be

measured with a similar accuracy and sensitively register smallest variations in the bonding structure of closely related molecules. Work is in progress to investigate how the approach presented here can be extended to labile systems, for which measured vibrational frequencies are not generally available. In this connection, it will be challenging to base a generally applicable AI exclusively on calculated vibrational frequencies. DFT results for a test set of 18 aromatic, nonaromatic, and antiaromatic molecules confirm this expectation. However, extension of this study to the coupled cluster level, inclusion of larger basis sets, and calculation of anharmonicity corrections for the vibrational frequencies are needed to have computationally reliable evidence for a generally applicable aromaticity/antiaromaticity index.

■ ASSOCIATED CONTENT

Ⓢ Supporting Information

ACS diagrams, normal mode decomposition tables, and diagrams of all molecules investigated. This material is available free of charge via the Internet at http://pubs.acs.org.

■ AUTHOR INFORMATION

Corresponding Author

*E-mail: dieter.cremer@gmail.com.

Notes

The authors declare no competing financial interest.

■ ACKNOWLEDGMENTS

■ REFERENCES

(1) Pauling, L. *The Nature of the Chemical Bond and the Structure of Molecules and Crystals, An Introduction to Modern Structural Chemistry*; Cornell University Press: Ithaca, NY, 1960.

(2) McWeeney, R. *Coulson's Valence*; Oxford University Press: Oxford, U.K., 1979.

(3) Kraka, E.; Cremer, D. In *Chemical Implication of Local Features of the Electron Density Distribution in Theoretical Models of Chemical Bonding: The Concept of the Chemical Bond*; Maksić, Z., Ed.; Springer: Heidelberg, 1990; Vol. 2, pp 453–542.

(4) Minkin, V. I.; Glukhovtsev, M. N.; Simkin, B. Y. *Aromaticity and Antiaromaticity: Electronic and Structural Aspects*; Wiley: New York, 1994.

(5) Randic, M. Aromaticity of Polycyclic Conjugated Hydrocarbons. *Chem. Rev.* **2003**, *103*, 3449–3605.

(6) Kertesz, M.; Choi, C. H.; Yang, S. Conjugated Polymers and Aromaticity. *Chem. Rev.* **2005**, *105*, 3448–3481.

(7) Chen, Z.; Wannere, C. S.; Corminboeuf, C.; Puchta, R.; Schleyer, P. v. R. Nucleus-Independent Chemical Shifts (NICS) as an Aromaticity Criterion. *Chem. Rev.* **2005**, *105*, 3842–3888.

(8) Mandado, M.; Moa, M. J. G.; Mosquera, R. A. *Aromaticity: Exploring Basic Chemical Concepts with the Quantum Theory of Atoms in Molecules*; Nova Science: New York, 2008.

(9) Gleiter, R.; Haberhauer, G. *Aromaticity and Other Conjugation Effects*; Wiley: New York, 2012.

(10) De Proft, F.; Geerlings, P. Conceptual and Computational DFT in the Study of Aromaticity. *Chem. Rev.* **2001**, *101*, 1451–1464.

(11) Cremer, D.; Kraka, E. From Molecular Vibrations to Bonding, Chemical Reactions, and Reaction Mechanism. *Curr. Org. Chem.* **2010**, *14*, 1524–1560.

(12) Cremer, D.; Gräfenstein, J. Calculation and Analysis of NMR Spin–spin Coupling Constants; Feature Article. *Phys. Chem. Chem. Phys.* **2007**, *9*, 2791–2816.

(13) Langhoff, S. R. Theoretical Infrared Spectra for Polycyclic Aromatic Hydrocarbon Neutrals, Cations, and Anions. *J. Phys. Chem.* **1996**, *100*, 2819–2841.

(14) Seahra, S.; Duley, W. Normal Coordinate Analysis and Vibrational Spectra of Aromatic Carbon Nanostructures. *Astrophys. J.* **2000**, *542*, 898–913.

(15) Andrews, L.; Moskovits, M. *Chemistry and Physics of Matrix-Isolated Species*; North-Holland: Amsterdam, 1989.

(16) Barone, V. Anharmonic Vibrational Properties By a Fully Automated Second-Order Perturbative Approach. *J. Chem. Phys.* **2005**, *122*, 014108-1–014108-10.

(17) Kjaergaard, H. G.; Garden, A. L.; Chaban, G. M.; Gerber, R. B.; Matthews, D. A.; Stanton, J. F. Calculation of Vibrational Transition Frequencies and Intensities in Water Dimer: Comparison of Different Vibrational Approaches. *J. Phys. Chem. A* **2008**, *112*, 4324–4335.

(18) Wilson, E. B.; Decius, J. C.; Cross, P. C. *Molecular Vibrations. The Theory of Infrared and Raman Vibrational Spectra*; McGraw-Hill: New York, 1955.

(19) Cremer, D.; Larsson, J. A.; Kraka, E. In *Theoretical and Computational Chemistry, Vol. 5, Theoretical Organic Chemistry*; Parkanyi, C., Ed.; Elsevier: Amsterdam, 1998; pp 259–327.

(20) Kraka, E.; Larsson, J. A.; Cremer, D. In *Computational Spectroscopy: Methods, Experiments and Applications*; Grunenberg, J., Ed.; Wiley: New York, 2010; pp 105–149.

(21) Shimanouchi, T. *Tables of Molecular Vibrational Frequencies Consolidated*; National Bureau of Standards: Gaithersburg, MD, 1972; Vol. *I*.

(22) Srivastava, A.; Singh, V. Theoretical and Experimental Studies of Vibrational Spectra of Naphthalene and Its Cation. *Ind. J. Pure Appl. Phys.* **2007**, *45*, 714–720.

(23) Räsänen, J.; Stenman, F.; Penttinen, E. Raman Scattering From Molecular Crystals—II. Anthracene. *Spectrochim. Acta Part A* **1973**, *29*, 395–403.

(24) Cyvin, B. N.; Cyvin, S. J. Mean Amplitudes of Vibration of Comparatively Large Molecules. III. Isotopic Anthracenes. *J. Phys. Chem.* **1969**, *73*, 1430–1438.

(25) Evans, D. J.; Scully, D. B. Non-Planar Vibration Frequencies of Anthracene. *Spectrochim. Acta* **1964**, *20*, 891–900.

(26) Bakke, A.; Cyvin, B. N.; Whitmer, J. C.; Cyvin, S. J.; Gustavsen, J. E.; Klaeboe, P. Z. Condensed Aromatics. Part II. The Five-Parameter Approximation of the In-Plane Force Field of Molecular Vibrations. *Naturforsch. Teil.* **1979**, *A34*, 579–584.

(27) Szczepanski, J.; Vala, M.; Talbi, D.; Parisel, O.; Ellinger, Y. Electronic and Vibrational Spectra of Matrix Isolated Anthracene Radical Cations: Experimental and Theoretical Aspects. *J. Chem. Phys.* **1993**, *98*, 4494–4511.

(28) Lee, S. Y.; Boo, B. H. Density Functional Theory Study of Vibrational Spectra of Anthracene Neutral and Radical Cation. *Bull. Korean Chem. Soc.* **1996**, *17*, 755–759.

(29) Bree, A.; Solven, F. G.; Vilkos, V. V. B. A Vibrational Analysis For Phenanthrene. *J. Mol. Spectrosc.* **1972**, *44*, 298–319.

(30) Konkoli, Z.; Cremer, D. A New Way of Analyzing Vibrational Spectra. I. Derivation of Adiabatic Internal Modes. *Int. J. Quantum Chem.* **1998**, *67*, 1–9.

(31) Zou, W.; Kalescky, R.; Kraka, E.; Cremer, D. Relating Normal Vibrational Modes To Local Vibrational Modes With The Help of an Adiabatic Connection Scheme. *J. Chem. Phys.* **2012**, *137*, 084114-1–084114-11.

(32) Zou, W.; Kalescky, R.; Kraka, E.; Cremer, D. Relating Normal Vibrational Modes To Local Vibrational Modes Benzene and Naphthalene. *J. Mol. Model.* **2012**, 1–13.

(33) Freindorf, M.; Kraka, E.; Cremer, D. A Comprehensive Analysis of Hydrogen Bond Interactions Based on Local Vibrational Modes. *Int. J. Quantum Chem.* **2012**, *112*, 3174–3187.

(34) Kalescky, R.; Zou, W.; Kraka, E.; Cremer, D. Local Vibrational Modes of the Water Dimer — Comparison of Theory and Experiment. *Chem. Phys. Lett.* **2012**, *554*, 243–247.

(35) Kalescky, R.; Kraka, E.; Cremer, D. Local Vibrational Modes of the Formic Acid Dimer − The Strength of the Double Hydrogen Bond. *Mol. Phys.* **2013**, *111*, 1497−1510.

(36) Kalescky, R.; Kraka, E.; Cremer, D. Identification of the Strongest Bonds in Chemistry. *J. Phys. Chem. A* **2013**, *117*, 8981−8995.

(37) Kruszewski, J.; Krygowski, T. Definition of Aromaticity Basing on the Harmonic Oscillator Model. *Tetrahedron Lett.* **1972**, *13*, 3839−3842.

(38) Krygowski, T. Crystallographic Studies of Inter- and Intra-molecular Interactions Reflected in Aromatic Character of π-Electron Systems. *J. Chem. Inf. Comput. Sci.* **1993**, *33*, 70−78.

(39) Krygowski, T. M.; Cyranski, M. Separation of the Energetic and Geometric Contributions to the Aromaticity. Part IV. A General Model for the π-Electron Systems. *Tetrahedron* **1996**, *52*, 10255−10264.

(40) Krygowski, T. M.; Cyranski, M. Structural Aspects of Aromaticity. *Chem. Rev.* **2001**, *101*, 1385−1420.

(41) Matta, C. F.; Hernández-Trujillo, J.; Tang, T.-H.; Bader, R. F. W. Hydrogen-Hydrogen Bonding: A Stabilizing Interaction in Molecules and Crystals. *Chem.—Eur. J.* **2003**, *9*, 1940−1951.

(42) Poater, P.; Visser, R.; Sola, M.; Bickelhaupt, F. M. Polycyclic Benzenoids: Why Kinked is More Stable than Straight. *J. Org. Chem.* **2007**, *72*, 1134−1142.

(43) Grimme, S.; Mück-Lichtenfeld, C.; Erker, G.; Kehr, G.; Wang, H.; Beckers, H.; H., W. When Do Interacting Atoms Form a Chemical Bond? Spectroscopic Measurements and Theoretical Analyses of Dideuteriophenanthrene. *Angew. Chem., Int. Ed.* **2009**, *48*, 2592−2595.

(44) Bader, R. F. W. Bond Paths Are Not Chemical Bonds. *J. Chem. Phys. A* **2009**, *113*, 10391−10396.

(45) Hancock, R.; Nikolayenko, I. V. Do Nonbonded H−H Interactions In Phenanthrene Stabilize It Relative To Anthracene? A Possible ·Resolution To This Question and Its Implications for Ligands Such As 2,2′-Bipyridyl. *J. Chem. Phys. A* **2012**, *116*, 8572−8583.

(46) Becke, A. D. Density-functional Thermochemistry. III. The Role of Exact Exchange. *J. Chem. Phys.* **1993**, *98*, 5648−5652.

(47) Stevens, P. J.; Devlin, F. J.; Chablowski, C. F.; Frisch, M. J. Ab Initio Calculation of Vibrational Absorption and Circular Dichroism Spectra Using Density Functional Force Fields. *J. Phys. Chem.* **1994**, *98*, 11623−11627.

(48) Dunning, T. H. Gaussian Basis Sets For Use In Correlated Molecular Calculations. I. The Atoms Boron Through Neon and Hydrogen. *J. Chem. Phys.* **1989**, *90*, 1007−1023.

(49) Kendall, R.; Dunning, T., Jr.; Harrison, R. J. Electron Affinities of the First-Row Atoms Revisited. Systematic Basis Sets and Wave Functions. *J. Chem. Phys.* **1992**, *96*, 6796−6806.

(50) Cremer, D.; Pople, J. A. General Definition of Ring Puckering Coordinates. *J. Am. Chem. Soc.* **1975**, *97*, 1354−1358.

(51) Cremer, D.; Szabo, K. J. In *Methods in Stereochemical Analysis, Conformational Behavior of Six-Membered Rings, Analysis, Dynamics, and Stereoelectronic Effects*; Juaristi, E., Ed.; VCH Publishers: New York, 1995; pp 59−133.

(52) Badger, R. M. A Relation Between Internuclear Distances and Bond Force Constants. *J. Chem. Phys.* **1934**, *2*, 128−132.

(53) Huber, K. P.; Herzberg, G. *Molecular Spectra and Molecular Structure, IV. Constants of Diatomic Molecules*; Van Nostrand Reinholdl: New York, 1979.

(54) Kawaguchi, K.; Hirota, E. Diode Laser Spectroscopy of the v_3 and v_3 Bands of FHF^- in 1300 cm^{-1} Region. *J. Chem. Phys.* **1987**, 6838−6841.

(55) Andrzejak, M.; Kubisiak, P.; Zborowski, K. K. Avoiding Pitfalls of a Theoretical Approach: The Harmonic Oscillator Measure of Aromaticity Index from Quantum Chemistry Calculations. *Struct. Chem.* **2013**, *24*, 1171−1184.

(56) Konkoli, Z.; Cremer, D. A New Way of Analyzing Vibrational Spectra. IV. Application and Testing of Adiabatic Modes Within the Concept of the Characterization of Normal Modes. *Int. J. Quantum Chem.* **1998**, *67*, 29−40.

(57) Kraka, E.; Filatov, M.; Zou, W.; Gräfenstein, J.; Joo, H.; Izotov, D.; Gauss, J.; He, Y.; Wu, A.; Cremer, D.; et al., *COLOGNE2013*; Southern Methodist University: Dallas, TX, 2013.

(58) Cox, J. D.; Pilcher, G. *Thermochemistry of Organic and Organometallic Compounds*; Academic Press: New York, 1970.

(59) Nagano, Y.; Nakano, M. Strain Energy of Phenanthrene. *J. Chem. Thermodyn.* **2003**, *35*, 1403−1412.

(60) Roux, M.; Temprado, M.; Chickos, J.; Nagano, Y. Critically Evaluated Thermochemical Properties of Polycyclic Aromatic Hydrocarbons. *J. Phys. Chem. Ref. Data* **2008**, *37*, 1855−1996.

(61) Ketkar, S. N.; Fink, M. The Molecular Structure of Naphthalene by Electron Diffraction. *J. Mol. Struct.* **1981**, *77*, 139−147.

(62) Almenmngen, A.; Bastiansen, G.; Dyvik, F. An Attempt to Determine the Structure Parameters of Condensed Ring Hydrocarbons Using the Electron Diffraction Method in Gas Molecules. *Acta Crystallogr.* **1961**, *14*, 1056−1065.

(63) Brock, C. P.; Dunitz, J. D. Temperature Dependence of Thermal Motion in Crystalline Naphthalene. *Acta Cryst. B* **1982**, *38*, 2218−2228.

(64) Ponomarev, V. I.; Filipenko, O. S.; Atovmyan, L. O. Crystal and molecular structure of naphthalene at −150 °C. *Sov. Phys. Cryst.* **1976**, *21*, 215−216.

(65) George, P.; Trachtman, M.; Bock, C. W.; Brett, A. L. Homodesmotic Reactions for the Assessment of Stabilization Energies in Benzenoid and Other Conjugated Cyclic Hydrocarbons. *J. Chem. Soc., Perkin Trans. 2* **1976**, *1976*, 1222−1227.

(66) Roth, W.; Adamczaka, O.; Breuckmann, R.; Lennartz, H.-W.; Boese, R. Die Berechnung von Resonanzenergien; das MM2ERW-Kraftfeld. *Chem. Ber.* **1991**, *124*, 2499−2521.

(67) Roth, W. R.; Frank-Gerrit Klarner, F.-G.; Siepert, G.; Lennartz, H.-W. Zur Frage der Homoaromatizitat von Norcaradien und Cycloheptatrien. *Chem. Ber.* **1992**, *125*, 217−224.

(68) Cremer, D.; E., K. A Description of the Chemical Bond in Terms of Local Properties of Electron Density and Energy, in Conceptual Approaches in Quantum Chemistry − Models and Applications. *Croatica Chem. Acta* **1984**, *57*, 1259−1281.

(69) Cremer, D.; E., K. Chemical Bonds without Bonding Electron Density - Does the Difference Electron Density Analysis Suffice for a Description of the Chemical Bond? *Angew. Chem., Int. Ed. Engl.* **1984**, *23*, 627−628.

(70) Pauling, L.; Sherman, J. The Nature of the Chemical Bond. VI. The Calculation from Thermochemical Data of the Energy of Resonance of Molecules Among Several Electronic Structures. *J. Chem. Phys.* **1933**, *1*, 606−617.

(71) Clar, E. *The Aromatic Sextet*; Wiley: New York, 1972.

(72) Steiner, E.; Fowler, P. W.; Havenith, R. W. A. Current Densities of Localized and Delocalized Electrons in Molecules. *J. Phys. Chem. A* **2002**, *106*, 7048−7056.

(73) Lazzeretti, P. In *Progress in Nuclear Magnetic Resonance Spectroscopy*; Emsley, J. W., Feeney, J., Sutcliffe, L. H., Eds.; Elsevier: Amsterdam, 2000; Vol. 36, pp 1−88.

(74) Ligabue, A.; Pincelli, U.; Lazzeretti, P.; Zanasi, R. Current Density Maps, Magnetizability, and Nuclear Magnetic Shielding Tensors for Anthracene, Phenanthrene, and Triphenylene. *J. Am. Chem. Soc.* **1999**, *121*, 5513−5518.

(75) Anusooya, Y.; Chakrabarti, A.; Pati, S. K.; Ramasesha, S. Ring Currents in Condensed Ring Systems. *Int. J. Quantum Chem.* **1998**, *70*, 503−513.

(76) Steiner, E.; Fowler, P. W. Ring Currents in Aromatic Hydrocarbons. *Int. J. Quantum Chem.* **1996**, *60*, 609−616.

(77) Dabestani, R.; Ivanov, I. N. A Compilation of Physical, Spectroscopic and Photophysical Properties of Polycyclic Aromatic Hydrocarbons. *Photochem. Photobiol.* **1999**, *70*, 10−34.

(78) Boschi, R.; Clar, E.; Schmidt, W. Photoelectron Spectra of Polynuclear Aromatics. III. The Effect of Nonplanarity in Sterically Overcrowded Aromatic Hydrocarbons. *J. Chem. Phys.* **1974**, *60*, 4406−4418.

(79) Biermann, D.; Schmidt, W. Diels−Alder Reactivity of Polycyclic Aromatic Hydrocarbons. 1. Acenes and Benzologs. *J. Am. Chem. Soc.* **1980**, *102*, 3163−3173.

(80) Biermann, D.; Schmidt, W. Diels−Alder Reactivity of Polycyclic Aromatic Hydrocarbons. 2. Phenes and Starphenes. *J. Am. Chem. Soc.* **1980**, *102*, 3173−3181.

236

dx.doi.org/10.1021/jp4092514 | *J. Phys. Chem. A* 2014, 118, 223−237

(81) Kato, T.; Yoshizawa, K.; Hirao, K. Electron−Phonon Coupling in Negatively Charged Acene- and Phenanthrene-Edge-Type Hydrocarbon Crystals. *J. Chem. Phys.* **2002**, *116*, 3420−3429.

(82) Cyranski, M. K.; Stepien, B. T.; Krygowski, T. M. Global and Local Aromaticity of Linear and Angular Polyacenes. *Tetrahedron* **2000**, *56*, 9663−9667.

(83) Behrens, S.; Köster, A. M.; Jug, K. Delocalization Energy of π Electrons as an Index for Aromaticity of Polycyclic Hydrocarbons. *J. Org. Chem.* **1994**, *59*, 2546−2551.

(84) Moyano, A.; Paniagua, J. C. The Performance of Aromaticity Indices. *Trends Org. Chem.* **1993**, *4*, 697−712.

(85) Moyano, A.; Paniagua, J. C. A Simple Approach for the Evaluation of Local Aromaticities. *J. Org. Chem.* **1991**, *56*, 1858−1866.

(86) Fukui, K. Role of Frontier Orbitals in Chemical Reactions. *Science* **1982**, *218*, 747−754.

(87) Balaban, A. T. Is Aromaticity Outmoded? *Pure Appl. Chem.* **1980**, *52*, 1409−1429.

(88) Bader, R. F. W. *Atoms in Molecules, A Quantum Theory*; Oxford University Press: Oxford, U.K., 1990.

(89) Cremer, D.; Gauss, J. Theoretical Determination of Molecular Structure and Conformation. 20. Reevaluation of the Strain Energies of Cyclopropane and Cyclobutane Carbon−Carbon and Carbon−Hydrogen Bond Energies, 1,3 Interactions, and Σ−Aromaticity. *J. Am. Chem. Soc.* **1986**, *108*, 7467−7477.